ADVANCED FUNCTIONAL MATERIALS
www.afm-journal.de

Materials Views
www.MaterialsViews.com

Carbonized Polyacrylonitrile-Stabilized SeS_x Cathodes for Long Cycle Life and High Power Density Lithium Ion Batteries

*Chao Luo, Yujie Zhu, Yang Wen, Jingjing Wang, and Chunsheng Wang**

A facile synthesis of selenium sulfide (SeS_x)/carbonized polyacrylonitrile (CPAN) composites is achieved by annealing the mixture of SeS_2 and polyacrylonitrile (PAN) at 600 °C under vacuum. The SeS_x molecules are confined by N-containing carbon (ring) structures in the carbonized PAN to mitigate the dissolution of polysulfide and polyselenide intermediates in carbonate-based electrolyte. In addition, formation of solid electrolyte interphase (SEI) on the surface of SeS_x/CPAN electrode in the first cycle further prevents polysulfide and polyselenide intermediates from dissolution. The synergic restriction of SeS_x by both CPAN matrix and SEI layer allows SeS_x/CPAN composites to be charged and discharged in a low-cost carbonate-based electrolyte ($LiPF_6$ in EC/DEC) with long cycling stability and high rate capability. At a current density of 600 mA g^{-1}, it maintains a reversible capacity of 780 mAh g^{-1} for 1200 cycles. Moreover, it retains 50% of the capacity at 60 mA g^{-1} even when the current density increases to 6 A g^{-1}. The superior electrochemical performance of SeS_x/CPAN composite demonstrates that it is a promising cathode material for long cycle life and high power density lithium ion batteries. This is the first report on long cycling stability and high rate capability of selenium sulfide-based cathode material.

1. Introduction

Lithium ion batteries which drive most portable electronics are promising energy storage devices for electric vehicles and smart grids.[1] To fulfill the large-scale application of lithium ion batteries, energy density and cycle life of current Li-ion batteries have to be improved.[2] Anode materials such as Si and Sn can provide theoretical capacities of 3579 mAh g^{-1} and 993 mAh g^{-1} respectively,[3,4] while the capacities of commercial $LiCoO_2$ (137 mAh/g) and $LiFePO_4$ (170 mAh g^{-1}) are much lower than counterpart anodes.[5–7] The energy density of current lithium ion batteries is mainly limited by cathode materials. Due to a high theoretical capacity of 1672 mAh g^{-1}, sulfur has been considered as the next generation cathode for high energy Li-ion batteries,[8–12] and it has attracted considerable research interest from both academy and industry. However, lithium sulfur batteries suffer from two major problems:[13] (1) low utilization of sulfur and poor power density due to the insulating property of sulfur and lithium sulfide; (2) the dissolution of polysulfide intermediates triggers severe shuttle reaction, resulting in rapid capacity fading during lithiation/delithiation process. Nevertheless, the dissolution of insulating polysulfide intermediates into electrolytes also allows full lithiation of sulfur, thus increasing the sulfur utilization and capacity. The current strategy to achieve both long cycling stability and high capacity is to use highly polysulfide-soluble electrolyte, but physically restrict dissolved polysulfides inside sulfur cathode to prevent shuttle reaction. The most effective method is to employ conductive porous carbon as a host to constrain polysulfide intermediates and enhance the conductivity of sulfur.[14,15]

Recently, selenium, the congener of sulfur, is introduced as the cathode material for lithium ion batteries due to its higher electrical conductivity than sulfur and its comparable volumetric capacity (3253 Ah L^{-1}) to sulfur (3467 Ah L^{-1}).[16–18] As demonstrated in our previous work, selenium impregnated mesoporous carbon composite exhibits excellent capacity retention that there is no capacity loss after 1000 deep charge/discharge cycles.[19] However, the mass capacity (480 mAh g^{-1}) of selenium, is lower than the mass capacity of sulfur (from 800 mAh g^{-1} to 1000 mAh g^{-1}). Since selenium possesses high cycling stability, but low reversible capacity, and sulfur has high reversible capacity, but poor cycling stability, it is desirable to develop a cathode material that combines the advantages of S and Se. As a consequence, selenium sulfide (SeS_2) has been explored as a cathode material for lithium ion batteries.[16,17]

Since SeS_2 has similar chemical properties with sulfur and selenium, it is believed that the method used to stabilize sulfur and selenium should be also effective for SeS_2. It was reported that PAN could react with sulfur at 300 °C to form

C. Luo, Dr. Y. Zhu, Y. Wen, Prof. C. Wang
Department of Chemical and Biomolecular Engineering
University of Maryland
College Park, Maryland 20742, USA
E-mail: cswang@umd.edu
J. Wang
Department of Chemistry and Biochemistry
University of Maryland
College Park, Maryland 20742, USA

DOI: 10.1002/adfm.201303909

© 2014 WILEY-VCH Verlag GmbH & Co. KGaA, Weinheim

a stable and conductive heterocyclic compound which could confine elemental sulfur and stabilize polysulfides.[20,21] When the carbonization temperature increases to 600 °C, the N-containing carbon (ring) structures in carbonized polyacrylonitrile (PAN) is able to constrain lithium sulfide species,[22] which further enhances the cycling stability and electronic conductivity. In this study, we synthesized SeS_x/CPAN composites by annealing the mixture of SeS_2 and PAN at 600 °C under vacuum. The x in SeS_x/CPAN is less than 2 due to the property difference between Se and S in high temperature of 600 °C. SeS_x is uniformly distributed in the carbonized PAN spheres with a particle size of 200 nm, and the carbonized PAN matrix can effectively confine lithium polysulfide and lithium polyselenide intermediates, thus improving the cycling stability of SeS_x/CPAN composites in commercial electrolyte ($LiPF_6$ in EC/DEC). The SeS_x/CPAN composite delivers a reversible capacity of 780 mAh g^{-1} at the current density of 600 mA g^{-1}, and maintains the capacity of 780 mAh g^{-1} for 1200 cycles. As the current density increased from 60 mA g^{-1} to 6 A g^{-1}, the capacity retains 50% of the capacity at 60 mA g^{-1}, demonstrating its exceptional rate capability. The superior electrochemical performance of SeS_x/CPAN composite is owing to synergic restriction of SeS_x by both CPAN matrix and SEI layer. This is the first report on detailed electrochemical performance of selenium sulfide cathode. Our results demonstrate that SeS_x/CPAN composite is a promising cathode material for long cycle life and high power density lithium ion batteries.

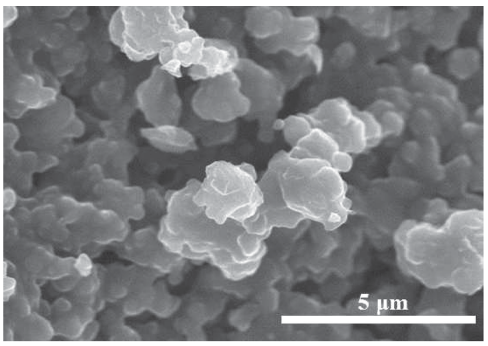

(a)

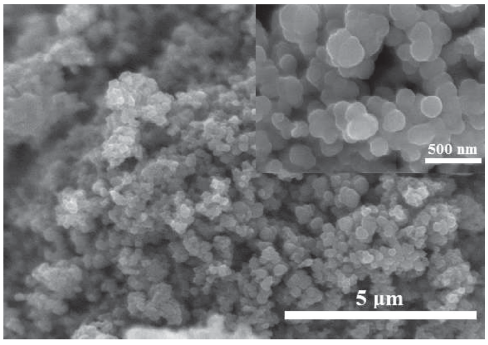

(b)

Figure 1. SEM images for PCPAN (a) and SeS_x/CPAN composites (b).

2. Results and Discussion

The scanning electron microscope (SEM) images in **Figure 1** show the morphology of pre-carbonized PAN (PCPAN) and SeS_x/CPAN composites. As shown in Figure 1(a), PCPAN synthesized under vacuum at a high temperature (600 °C) consists of irregular-shape particles with a size about 3 µm. The SeS_x/CPAN composites, synthesized by annealing the mixture of SeS_2 and PAN (1:1 by weight) at the same temperature of 600 °C under vacuum, are composed of round-shape particles with a small particle size of 200 nm. The morphology difference is attributed to the reaction between PAN and SeS_2. SeS_2 can dehydrogenate PAN to form a conductive main chain, in the meanwhile, –CN functional groups in PAN are cyclized to form a stable heterocyclic ring at the high temperature.[20] The heterocyclic ring can confine SeS_x and accommodate the volume change caused by the lithiation/delithiation. The transmission electron microscopy (TEM) image of SeS_x/CPAN composites (**Figure 2**a) shows that primary particles are in round-shape with a size about 200 nm, and these particles aggregate into a large cluster, which is consistent with the SEM images. High resolution transmission electron microscopy (HRTEM) and selected area electron diffraction (SAED) are also carried out to investigate the microstructure of the SeS_x/CPAN composite. From the HRTEM image and SAED pattern in Figure S1, it can be clearly observed that SeS_x/CPAN composite has an amorphous structure. The energy-dispersive X-ray spectroscopy (EDS) elemental mapping images in Figure 2b–d reveal that the carbon elemental mapping image overlaps with sulfur and selenium mapping images, demonstrating the uniform distribution of SeS_x in the carbon matrix. Moreover, the EDS mapping also indicates that the ratio of selenium and sulfur is 1:0.7, as shown in Figure S2, so x is 0.7. The content of $SeS_{0.7}$ in the $SeS_{0.7}$/CPAN composites is 33% as shown in the thermogravimetric analysis (TGA) in Figure S3.

The phase structure of $SeS_{0.7}$/CPAN composites was investigated by X-ray diffraction and Raman spectroscopy. **Figure 3**a and b show the XRD pattern and Raman spectrum of $SeS_{0.7}$/CPAN composites. XRD patterns and Raman spectra of pristine SeS_2 and PCPAN are also showed in Figure 3 as controls. The XRD pattern shows that $SeS_{0.7}$/CPAN composite has an amorphous structure, while pristine SeS_2 possesses a crystal structure. One broad peak at 26 degree in the XRD pattern of $SeS_{0.7}$/CPAN composites is attributed to the carbon matrix formed through carbonization of PAN. The amorphous structure of $SeS_{0.7}$ in $SeS_{0.7}$/CPAN composite may be due to the uniform distribution of $SeS_{0.7}$ at a molecular level in CPAN matrix, leading to strong confinement of $SeS_{0.7}$ in CPAN. Similar to the XRD pattern, characteristic Raman peaks of SeS_2 are not observed in $SeS_{0.7}$/CPAN composites, and only two broad carbon peaks at 1345 cm^{-1} and 1595 cm^{-1} representing the disordered graphite (D band) and crystalline graphite (G band), respectively, appear in the Raman spectrum of $SeS_{0.7}$/CPAN composites. Both XRD and Raman measurements confirm that $SeS_{0.7}$ molecules are constrained by CPAN to form an amorphous structure. The X-Ray Photoelectron Spectroscopy (XPS) analysis was also used to obtain valuable information about the surface of $SeS_{0.7}$/CPAN composites. The peaks for carbon-carbon bond and carbon-nitrogen bond are observed in Figure 3c. Since CPAN consists of well-formed N-containing

© 2014 WILEY-VCH Verlag GmbH & Co. KGaA, Weinheim

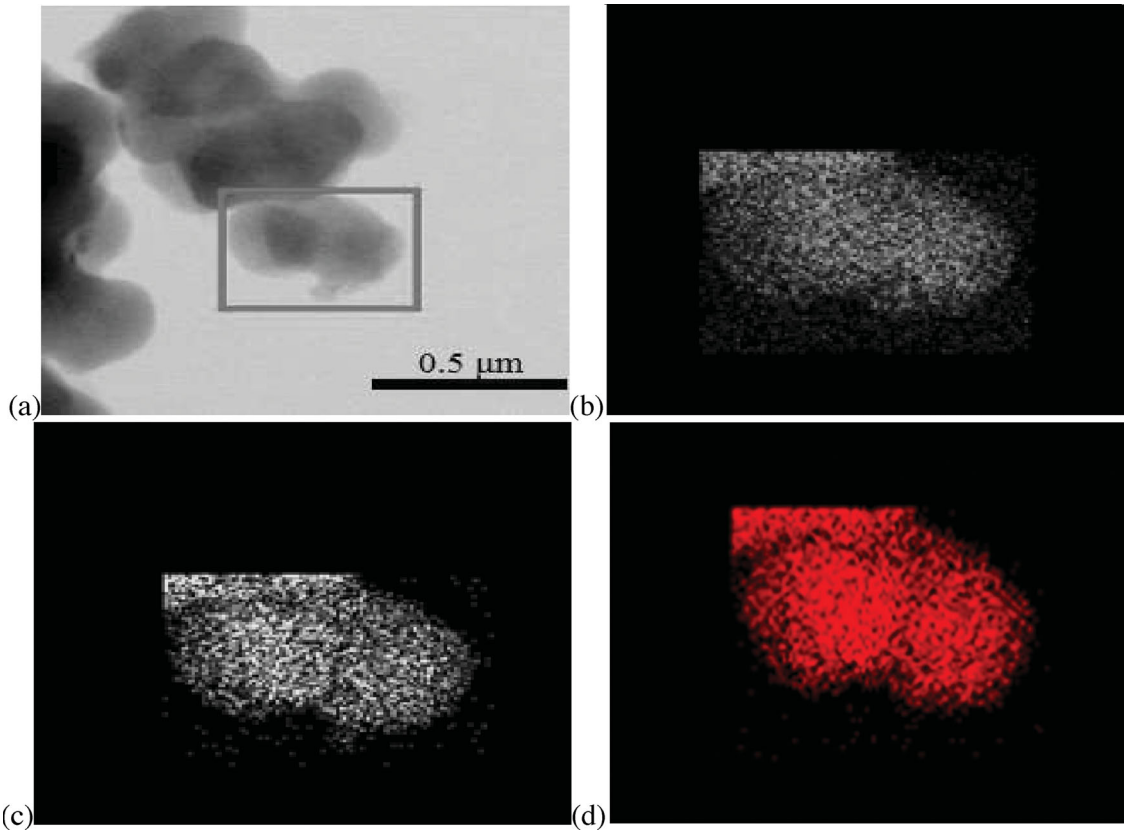

Figure 2. TEM image of SeS_x/CPAN composites (a) and EDS elemental mapping images of the SeS_x/CPAN composites, marked by a square, for carbon (b), sulfur (c) and selenium (d).

carbon (ring) structures,[23] the C 1s XPS spectrum is in well agreement with the structure of CPAN. The S 2p and Se 3p XPS spectrum in Figure 3d shows the XPS peaks for S 2p 1/2, S 2p 3/2, Se 3p 1/2 and Se 3p 3/2, which further confirms the existence of selenium sulfide in $SeS_{0.7}$/CPAN composites. Moreover, the composition of $SeS_{0.7}$ is obtained from the peak fit using relative sensitivity factors from the Kratos vision library, and atomic ratio of S to Se is calculated to be 0.7, which is coincident with the result of EDS analysis. It was reported that sulfur can react with selenium to generate selenium sulfide at a high temperature.[24,25] Moreover, the heterocyclic sulfur-selenium molecules such as Se_5S_2, Se_5S_3 and Se_3S_2 do exist as ring molecules with a majority of Se atoms.[26] Therefore, in the $SeS_{0.7}$/CPAN composite, $SeS_{0.7}$ can exist as molecules in the frame of CPAN.

The galvanostatic charge–discharge behaviors of $SeS_{0.7}$/CPAN composites in $LiPF_6$-EC/DEC electrolyte are shown in **Figure 4**a. During the first lithiation, a small plateau at 2.35 V and a long flat plateau at 1.7 V are observed. However, the short plateau at 2.35 V disappears, while the flat plateau at 1.7 V becomes a little steeper and shifts to 1.8 V in the subsequent cycles. The plateau at 2.35 V is assigned to the conversion of $SeS_{0.7}$ to polysulfides/polysenelides and the plateau at 1.7–1.8 V is atributed to conversion of polysulfides to Li_2S and polyselenides to Li_2Se.[17] The disappearence of the small plateau at 2.35 V is probably owing to the dissolution of high-order polysulfide/polyselenide intermediates into the electrolyte.[17] The long sloping line from 1.5 V to 0.8 V in the first lithiation becomes much steeper in the following lithiation cycles, resulting in large irreversible capacity in the first cycle. The large irreversible capacity induced at the potential range from 1.5 V to 0.8 V may be attributed to the formation of SEI layer on the surface of electrode. The low Coulombic efficiency (~58%) in the first cycle quickly increases to 95% in the second cycle, suggesting that SEI layer is well-formed after the first cycle. The SEI layer on $SeS_{0.7}$/CPAN electrode can prevent polysulfides/polysenelides from reacting with carbonate-based electrolyte. Similar SEI formation process is also observed in carbon black electrode. As shown in Figure S4, a long potential plateau between 1.0 V and 0.8 V in carbon black electrode is observed in the first cycle, but it disappears in the second cycle, resulting in a large irreversible capacity. The large irreversible capacity is ascribed to the formation and growth of SEI layer on the surface of carbon black, which is coincident with the result of $SeS_{0.7}$/CPAN electrode. During delithation, only one sloping plateau centered at 2.1 V can be observed, and this peak remains stable during following lithiation/delithiation cycles. The CV curves in Figure 4b are consistent with the charge–discharge curves. In the first scan, there are a small cathodic peak at 2.45 V, a sharp cathodic peak at 1.5 V and an anodic peak at 2.2 V. The small peak at 2.45 V dissappears after the first scan, while the sharp peak at 1.5 V shifts to 1.75 V in the subsequent scans. The peak shift indicates that there is an activation process due to volume expansion of $SeS_{0.7}$ in the first lithiation process,

© 2014 WILEY-VCH Verlag GmbH & Co. KGaA, Weinheim

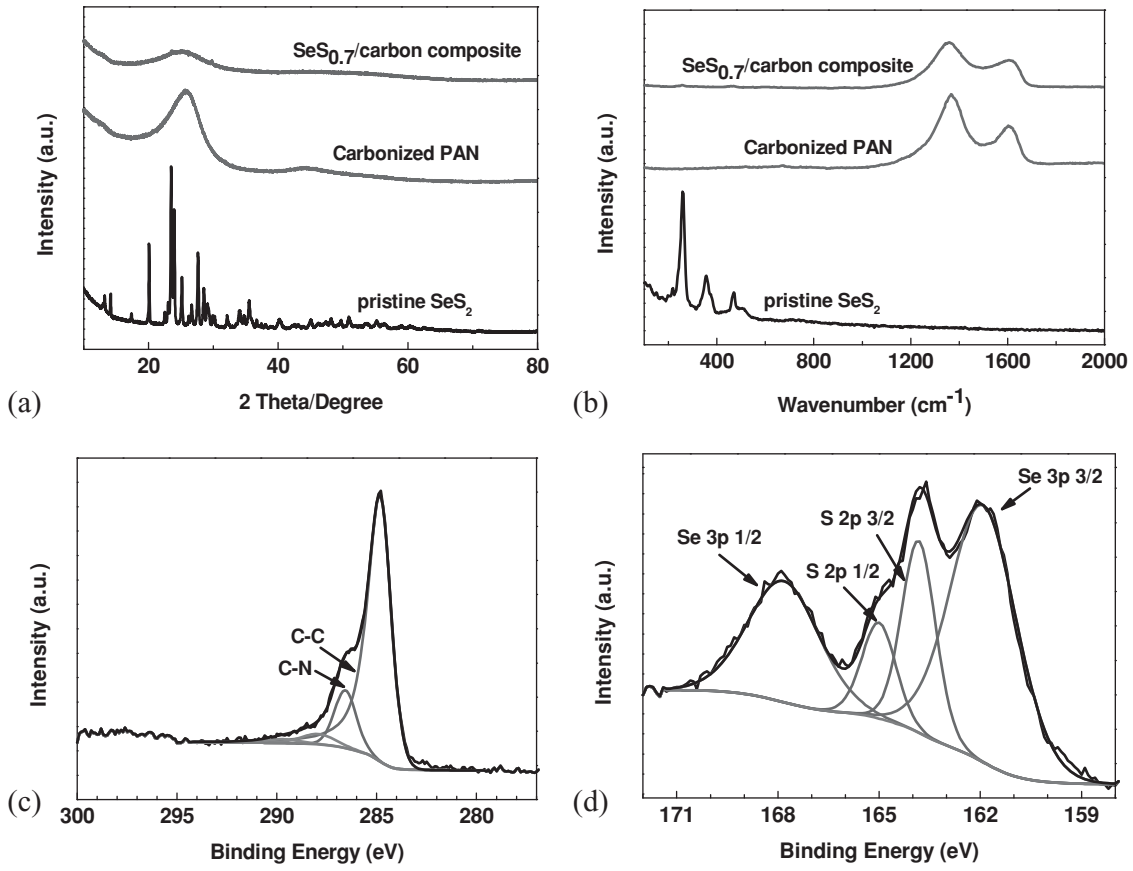

Figure 3. XRD patterns (a) and Raman spectra (b) for pristine SeS_2, PCPAN and $SeS_{0.7}$/CPAN composites; XPS spectra of $SeS_{0.7}$/CPAN composites: (c) C 1s, (d) S 2p, and Se 3p.

and then the peaks become very stable, demonstrating high cycling stability of $SeS_{0.7}$/CPAN composites. Figure 4c shows the cycling stability of $SeS_{0.7}$/CPAN composites. It delivers a reversible capacity of 780 mAh g^{-1}, and retains for 1200 cycles. The Coulombic efficiency of $SeS_{0.7}$/CPAN electrode is nearly 100%. Its high reversible capacity, long cycle life and high Coulombic efficiency demonstrate that CPAN can effectively confine $SeS_{0.7}$ and stabilize polysulfide and polyselenide intermediates. The rate performance of $SeS_{0.7}$/CPAN composite is shown in Figure 4d. At a current density of 60 mA g^{-1}, its reversible capacity can reach 900 mAh g^{-1}. As the current density increases from 60 mA g^{-1} to 6 A g^{-1}, the reversible capacity retains about 50% of the capacity at 60 mA g^{-1}. With the current density increased to 12 A g^{-1}, the capacity decreases to 80 mAh g^{-1}, but the reversible capacity recovers to 900 mAh g^{-1} after the current density returns to 60 mA g^{-1}, demonstrating its superior robustness to tolerate current changes. The excellent electrochemical performance of $SeS_{0.7}$/CPAN composites demonstrates that CPAN is a good carbon host to enhance the kinetics and cycling stability of $SeS_{0.7}$ cathode material. Therefore, the $SeS_{0.7}$/CPAN composite is a promising alternative to sulfur for long cycle life and high power density lithium ion batteries.

It was reported that selenide anions can react with the carbonyl groups in the carbonate solvent and form an insulating SEI layer on the cathode surface.[16,17] The SEI layer on Se/C cathode continuesly grows during charge/dishcarge cycles, reducing the cycling stability of Se/C cathode. On the contrary, $SeS_{0.7}$/CPAN electrode shows exceptional cycling stability in carbonate-based electrolyte. To investigate the mechanism behind the long cycle life, XPS, a surface-sensitive spectroscopic technique, was employed to obtain the SEI information on $SeS_{0.7}$/CPAN electrode at a fully charged state (3.0 V) after the 1st deep charge/discharge cycle. To remove $LiPF_6$ salt, cycled $SeS_{0.7}$/CPAN electrode was immersed in propylene carbonate for 48 h before XPS analysis. A control experiment was carried out with a fresh $SeS_{0.7}$/CPAN electrode. As shown in **Figure 5**, the XPS peaks for Na and N, resulting from sodium alginate binder and CPAN matrix, are clearly observed in the fresh $SeS_{0.7}$/CPAN electrode, but disappear in cycled $SeS_{0.7}$/CPAN electrode. The sulfur peaks cannot be observed in both fresh and cycled $SeS_{0.7}$/CPAN electrodes because the sulfur peaks overlap with selenium peaks in XPS spectrum. The disappearance of peaks for Na and N in cycled $SeS_{0.7}$/CPAN electrode is attributed to the formation of SEI layer on the surface of $SeS_{0.7}$/CPAN electrode that covers the sodium alginate binder and CPAN matrix. XPS is a surface-sensitive technique (10 nm). If $SeS_{0.7}$/CPAN electrode was covered by SEI layer, XPS cannot detect the material inside $SeS_{0.7}$/CPAN electrode, resulting in the disappearance of XPS peaks for Na and N. The formation of an insulating layer on the surface of Se cathode in carbonate-based electrolyte after the 1st cycle was also reported

© 2014 WILEY-VCH Verlag GmbH & Co. KGaA, Weinheim

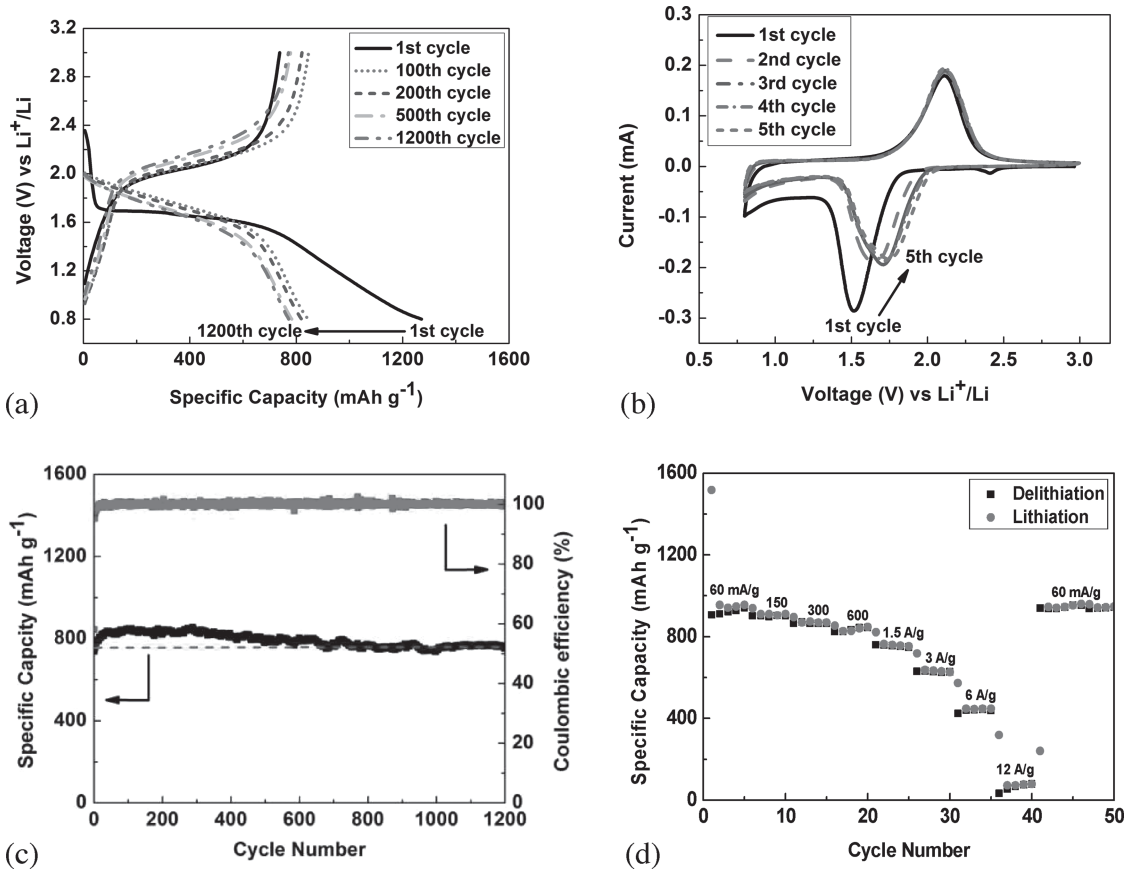

Figure 4. Electrochemical performance of $SeS_{0.7}$/CPAN composites. (a) The galvanostatic charge–discharge curves between 0.8 V and 3.0 V versus Li/Li^+; (b) cyclic voltammograms at 0.1 mV s^{-1} in the potential window from 0.8 V to 3.0 V versus Li/Li^+; (c) delithiation capacity and coulombic efficiency versus cycle number at the current density of 600 mA g^{-1}; (d) rate performance at various C-rates.

by Dr. Amine's group.[16,17] To further investigate the role of SEI layer in $SeS_{0.7}$/CPAN electrodes, LiTFSI-TEGDME is employed as an electrolyte in $SeS_{0.7}$/CPAN coin cells, because TEGDME solvent in LiTFSI-TEGDME electrolyte is stable and will not be reduced to form SEI layer during the lithiation process.[27] As shown in Figure S5, $SeS_{0.7}$/CPAN electrode in LiTFSI-TEGDME electrolyte suffers from quick capacity decline comparing to the highly stable cycling behavior of $SeS_{0.7}$/CPAN electrode in carbonate-based electrolyte. Moreover, the Coulombic efficiency (calculated based on lithiation capacity over delithiation capacity) in the initial 40 cycles is larger than 100% due to the dissolution of polysulfides and polyselenides. It demonstrates that CPAN matrix cannot effectively confine polysulfides and polyselenides without a stable SEI layer. Therefore, though the formation of SEI layer induces a large irreversible capacity in the first lithiation/delithiation cycle of $SeS_{0.7}$/CPAN electrode (Figure 4a), it can prevent the $SeS_{0.7}$ from reacting with carbonate-based electrolyte, leading to the enhancement of cycling stability.

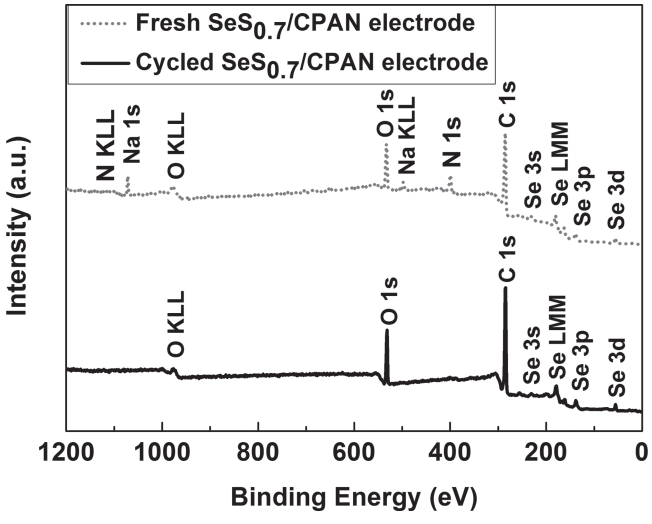

Figure 5. XPS spectrum of fresh $SeS_{0.7}$/CPAN electrode and cycled $SeS_{0.7}$/CPAN electrode.

The highly stable SEI layer during charge/discharge cycles was confirmed by electrochemical impedance spectroscopy (EIS). As shown in **Figure 6**, the impedance curve of fresh $SeS_{0.7}$/CPAN cathodes exhibits two depressed semi-circles in the high and middle frequency regions, and a sloping line in the low frequency region. The two depressed semicircles in the high and middle frequency regions merge into a single depressed semicircle after first charge/discharge cycle, and it remains stable during the rest of cycles. The high-frequency semicircle stands for contact resistance of $SeS_{0.7}$/CPAN

© 2014 WILEY-VCH Verlag GmbH & Co. KGaA, Weinheim

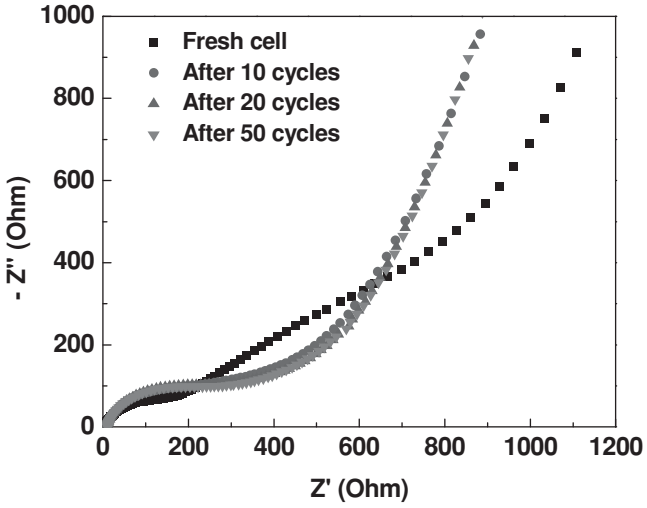

Figure 6. Impedance analysis for $SeS_{0.7}$/CPAN cell before test and after fully charge to 3.0 V and rest for 2 h.

particles in fresh $SeS_{0.7}$/CPAN cathode, and sum of SEI layer resistance and particle-to-particle resistance for cycled $SeS_{0.7}$/CPAN cathode. The middle-frequency semicircle is attributed to charge transfer resistance. The low frequency line represents ion diffusion resistance in the $SeS_{0.7}$/CPAN particles. The fresh $SeS_{0.7}$/CPAN cell displays a large charge transfer resistance and ion diffusion resistance due to limit access of liquid electrolyte into $SeS_{0.7}$/CPAN electrode film. After volume expansion/shrinkage in the first cycle, more electrolytes can penetrate into electrode film, leading to lower charge transfer resistance and shorter ion diffusion distance in the following cycles. The reduced impedance in the second cycle decreases the overpotential, and shifts the lithiation potential to a higher value as demonstrated in the CV curves in Figure 4b. The slightly impedance increase in the high-frequency semicircle is attributed to the formation of SEI layer. However, the formed SEI layer is very stable during following charge/discharge cycles, as evidenced by the overlapped impedance curves. The low and stable resistance of SEI layer and charge transfer reaction is coincident with the exceptional rate capability of $SeS_{0.7}$/CPAN composites (in Figure 4d), demonstrating its fast kinetics.

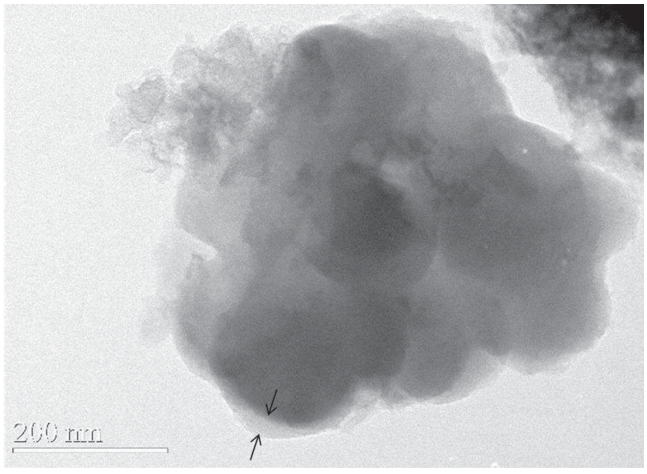

Figure 7. TEM image of the $SeS_{0.7}$/CPAN electrode after 100 cycles in Li-ion batteries.

The morphology change of $SeS_{0.7}$/CPAN composites during 100 deep charge/discharge cycles was studied by using TEM. From the TEM image in **Figure 7**, it can be observed that the cycled $SeS_{0.7}$/CPAN composites still consist of round-shape particles with a size about 200 nm, which is similar to the fresh $SeS_{0.7}$/CPAN composites (Figure 2a). It demonstrates that $SeS_{0.7}$/CPAN composites maintain the morphology after 100 cycles, and the good morphology maintenance guarantees high cycling stability of $SeS_{0.7}$/CPAN composites. The rough surface of the $SeS_{0.7}$/CPAN particles is due to formation of the SEI layer. As shown in Figure 7, A ~20 nm SEI layer can be observed on the surface of $SeS_{0.7}$/CPAN electrode after 100 cycles in $LiPF_6$-EC/DEC electrolyte. Moreover, the fuzzy SEI image of cycled $SeS_{0.7}$/CPAN in Figure S6 is attributed to the low electronic conductivity of SEI layer. Figure S7 shows the TEM image of $SeS_{0.7}$/CPAN electrode after first cycle in LiTFSI-TEGDME electrolyte. A clean surface of $SeS_{0.7}$/CPAN electrode without SEI layer is observed. To further confirm that SEI layer is not formed on this electrode, TEM EDX mapping is employed to check the elemental distribution of this electrode. As shown in Figure S8, C, S and Se can still be observed in the cycled electrode, but F which is a main component of SEI layer cannot be observed, demonstrating that SEI layer is not formed on electrodes in LiTFSI-TEGDME electrolyte. The elemental distribution in carbon black and binder (Sodium alginate), surrounding $SeS_{0.7}$/CPAN spheres, is also investigated by TEM EDX. As shown in Figure S9, C, S and Se are observed in the outside of $SeS_{0.7}$/CPAN spheres. The C peak results from carbon black and binder. The S and Se peaks result from the dissolution of polysulfides and polyselenides in LiTFSI-TEGDME electrolyte, which triggers the shuttle effect. F peak is not observed, further demonstrating the absence of SEI layer.

To investigate how the in-situ carbonization of PAN affects the cycling stability, the electrochemical performance of ex-situ carbonized SeS_2/pre-carbonized PAN (PCPAN) composite and pristine SeS_2 was also measured as controls to compare with in-situ formed $SeS_{0.7}$/CPAN composite. The SeS_2/PCPAN composite was synthesized by pre-carbonization of PAN (PCPAN in Figure 1a), and then infusing SeS_2 into PCPAN under the same condition as $SeS_{0.7}$/CPAN composite. TG analysis shows that only 13% of SeS_2 is infused into PCPAN (Figure S10), which is much lower than the content (33%) of $SeS_{0.7}$ in in-situ formed $SeS_{0.7}$/CPAN composite. The low SeS_2 content in ex-situ formed SeS_2/PCPAN composite is because the well-formed N-containing carbon (ring) structures in PCPAN hinder the diffusion of SeS_2 into carbonized PAN matrix. The first lithiation/delithiation curves of SeS_2/PCPAN composites in Figure S11 (a) exhibit higher overpotential and larger irreversible capacity (~62%) than $SeS_{0.7}$/CPAN composite (Figure 4a). The charge/discharge potential of ex-situ formed SeS_2/PCPAN in the following charge/discharge cycles is also slightly lower than that of in-situ formed $SeS_{0.7}$/CPAN. The reversible capacity of $SeS_{0.7}$/PCPAN composite is 1050 mAh g^{-1}, which is higher than that of $SeS_{0.7}$/CPAN composite. As shown in Figure S11 (b), SeS_2/PCPAN composite also exhibits excellent cycling stability. Although ex-situ formed SeS_2/PCPAN composite can maintain

© 2014 WILEY-VCH Verlag GmbH & Co. KGaA, Weinheim

reversible capacity of 1050 mAh g^{-1} for 700 cycles, the low SeS_2 content significantly reduces the overall capacity. Therefore, the in-situ formed $SeS_{0.7}$/CPAN composite is a more advanced cathode material than ex-situ formed SeS_2/PCPAN composite. As another control, the pristine SeS_2 electrode (Figure S12a) shows much worse battery performance than both in-situ formed $SeS_{0.7}$/CPAN and ex-situ formed SeS_2/PCPAN electrodes. It delivers high irreversible capacity (~70%) and low lithiation capacity in the first cycle due to the low conductivity of SeS_2. Nevertheless, the formation of SEI layer stabilizes the pristine SeS_2 and increases the Coulombic efficiency to almost 100% by preventing the shuttle reaction.

The effect of SEI layer on preventing the shuttle reaction was investigated by comparing the charge/discharge behaviors of pristine SeS_2 in carbonate-based electrolyte and LiTFSI-TEGDME electrolyte. The sloping lithiation plateau of pristine SeS_2 in $LiPF_6$-EC/DEC electrolyte centered at 1.7 V shifts to flat plateaus centered at 2.0 V in LiTFSI-TEGDME electrolyte (Figure S12b). LiTFSI-TEGDME is a standard electrolyte for S and SeS_2 cathodes because it does not react with polysulfides/polyselenides.[16,17] The reversible capacity of pristine SeS_2 in LiTFSI-TEGDME electrolyte continuously decreases from 1st cycle to 10th cycle, while its reversible capacity in $LiPF_6$-EC/DEC electrolyte remains stable after the first cycle. Thus, the SEI layer formed in carbonate-based electrolyte stablizes the SeS_2 electrode and increases the Coulombic efficiency.

3. Conclusion

The $SeS_{0.7}$/CPAN composites were synthesized by annealing the mixture of SeS_2 and PAN at 600 °C under vacuum. The CPAN matrix can enhance the electrical conductivity of $SeS_{0.7}$ material and constrain the polysulfide and polyselenide intermediates during the lithiation/delithiation process, leading to superior electrochemical performance of $SeS_{0.7}$/CPAN composites. The formation of stable SEI layer on the surface of $SeS_{0.7}$/CPAN electrode further contributes to the long cycle life and high Coulombic efficiency. The composite delivers a reversible capacity of 780 mAh g^{-1} and retains for 1200 cycles. As the current density increases from 60 mA g^{-1} to 6 A g^{-1}, its capacity retention is about 50%, demonstrating its high rate capability. Therefore, $SeS_{0.7}$/CPAN composite is a promising cathode material for long cycle life and high power density lithium ion batteries.

4. Experimental Section

Synthesis of $SeS_{0.7}$/CPAN Composites: All chemicals were purchased from Sigma Aldrich and used as received. Selenium sulfide and polyacrylonitrile were mixed with a ratio of 1:1 by weight and sealed in a glass tube under vacuum. The sealed glass tube was annealed in an oven at 600 °C for 3 h, and it was cooled to room temperature in 24 h. $SeS_{0.7}$/CPAN composites were collected as black powder. PCPAN is also synthesized in a sealed glass tube at 600 °C for 3 h in vacuum.

Material Characterizations: Scanning electron microscopy (SEM) images were taken by Hitachi SU-70 analytical ultra-high resolution SEM (Japan); Transmission electron microscopy (TEM) images were taken by JEOL (Japan) 2100F field emission TEM; Thermogravimetric analysis (TGA) was carried out using a thermogravimetric analyzer (TA Instruments, USA) with a heating rate of 10 °C min^{-1} in argon; X-ray diffraction (XRD) pattern was recorded by Bruker Smart1000 (Bruker AXS Inc., USA) using CuKα radiation; Raman measurements were performed on a Horiba Jobin Yvon Labram Aramis using a 532 nm diode-pumped solid-state laser, attenuated to give ~900 μW power at the sample surface. The X-Ray Photoelectron Spectroscopy (XPS) analysis was performed on a high sensitivity Kratos AXIS 165 X-ray Photoelectron Spectrometer using monochronic Al Kα radiation.

Electrochemical Measurements: The $SeS_{0.7}$/CPAN composites were mixed with carbon black and sodium alginate binder to form a slurry at the weight ratio of 80:10:10. The electrode was prepared by casting the slurry onto aluminum foil using a doctor blade and dried in a vacuum oven at 60 °C overnight. The slurry coated on aluminum foil was punched into circular electrodes with an area mass loading of 1.2 mg cm^{-2}. The same method is used to fabricate pristine selenium sulfide electrode and carbon black electrode. The pristine selenium sulfide electrode was made by mixing selenium sulfide, carbon black and sodium alginate binder at a weight ratio of 26:64:10. The carbon black electrode was made by mixing carbon black and sodium alginate binder at a weight ratio of 90:10. Coin cells for lithium selenium sulfide batteries were assembled with lithium foil as the counter electrode, 1M $LiPF_6$ in a mixture of ethylene carbonate/diethyl carbonate (EC/DEC, 1:1 by volume) or 1M LiTFSI in tetraethylene glycol dimethyl ether (TEGDME) as the electrolyte, and Celgard®3501 (Celgard, LLC Corp., USA) as the separator. Electrochemical performance was tested using Arbin battery test station (BT2000, Arbin Instruments, USA). Capacity was calculated on the basis of the mass of selenium sulfide in $SeS_{0.7}$/CPAN composites. Cyclic voltammograms were recorded using Gamry Reference 3000 Potentiostat/Galvanostat/ZRA with a scan rate of 0.1 mV s^{-1}. Impedance analysis was also performed by Gamry Reference 3000 Potentiostat/Galvanostat/ZRA.

Supporting Information

Supporting Information is available from the Wiley Online Library or from the author.

Acknowledgements

This work was supported by the Army Research Office under Contract No.: W911NF1110231. We acknowledge the support of the Maryland NanoCenter and its NispLab. The NispLab is supported in part by the NSF as a MRSEC Shared Experimental Facility. We acknowledge Kaitlyn Crawford, Prof. Lawrence R. Sita and Dr. Karen Gaskell for their technique support.

Note: Figure 2d was replaced with a colour version and the caption was corrected after initial online publication.

Received: November 20, 2013
Revised: January 19, 2014
Published online: March 20, 2014

[1] B. Scrosati, J. Hassounab, Y. Sun, *Energy Environ. Sci.* **2011**, *4*, 3287.
[2] J. B. Goodenough, Y. Kim, *Chem. Mater.* **2010**, *22*, 587.
[3] U. Kasavajjula, C. Wang, A. J. Appleby, *J. Power Sources* **2007**, *163*, 1003.
[4] Y. Xu, Q. Liu, Y. Zhu, Y. Liu, A. Langrock, M. R. Zachariah, C. Wang, *Nano Lett.* **2013**, *13*, 470.
[5] B. L. Ellis, K. T. Lee, L. F. Nazar, *Chem. Mater.* **2010**, *22*, 691.
[6] B. Kang, G. Ceder, *Nature* **2009**, *458*, 190.
[7] Y. Zhu, Y. Xu, Y. Liu, C. Luo, C. Wang, *Nanoscale* **2013**, *5*, 780.
[8] P. G. Bruce, S. A. Freunberger, L. J. Hardwick, J. Tarascon, *Nat. Mater.* **2012**, *11*, 19.
[9] J. Guo, Y. Xu, C. Wang, *Nano Lett.* **2011**, *11*, 4288.
[10] Z. Lin, Z. Liu, W. Fu, N. J. Dudney, C. Liang, *Adv. Funct. Mater.* **2013**, *23*, 1064.

© 2014 WILEY-VCH Verlag GmbH & Co. KGaA, Weinheim

[11] J. Kim, D. Lee, H. Jung, Y. Sun, J. Hassoun, B. Scrosati, *Adv. Funct. Mater.* **2013**, *23*, 1076.
[12] J. Song, T. Xu, M. L. Gordin, P. Zhu, D. Lv, Y. Jiang, Y. Chen, Y. Duan, D. Wang, *Adv. Funct. Mater.* **2013**, DOI: 10.1002/adfm.201302631.
[13] D. Wang, Q. Zeng, G. Zhou, L. Yin, F. Li, H. Cheng, I. R. Gentle, G. Q. Lu, *J. Mater. Chem. A* **2013**, *1*, 9382.
[14] X. Ji, K. T. Lee, L. F. Nazar, *Nat. Mater.* **2009**, *8*, 500.
[15] B. Zhang, X. Qin, G. R. Li, X. P. Gao, *Energy Environ. Sci.* **2010**, *3*, 1531.
[16] A. Abouimrane, D. Dambournet, K. W. Chapman, P. J. Chupas, W. Weng, K. Amine, *J. Am. Chem. Soc.* **2012**, *134*, 4505.
[17] Y. Cui, A. Abouimrane, J. Lu, T. Bolin, Y. Ren, W. Weng, C. Sun, V. A. Maroni, S. M. Heald, K. Amine, *J. Am. Chem. Soc.* **2013**, *135*, 8047.
[18] C. Yang, S. Xin, Y. Yin, H. Ye, J. Zhang, Y. Guo, *Angew. Chem. Int. Ed.* **2013**, *52*, 8363.
[19] C. Luo, Y. Xu, Y. Zhu, Y. Liu, S. Zheng, Y. Liu, A. Langrock, C. Wang, *ACS Nano* **2013**, *7*, 8003.
[20] J. Wang, J. Yang, C. Wan, K. Du, J. Xie, N. Xu, *Adv. Funct. Mater.* **2003**, *13*, 487.
[21] L. Yin, J. Wang, F. Lin, J. Yang, Y. Nuli, *Energy Environ. Sci.* **2012**, *5*, 6966.
[22] J. Guo, Z. Yang, Y. Yu, H. D. Abruña, L. A. Archer, *J. Am. Chem. Soc.* **2013**, *135*, 763.
[23] M.S.A. Rahaman, A. F. Ismail, A. Mustafa, *Polym. Degrad. Stab.* **2007**, *92*, 1421.
[24] R. Laitinen, T. Pakkanen, *J. Mol. Struct.: THEOCHEM* **1983**, *91*, 337.
[25] J. Drowart, S. Smoes, *J. Chem. Soc., Faraday Trans.* **1977**, *73*, 1755.
[26] R. O. Jones, D. Hohl, *J. Am. Chem. Soc.* **1990**, *112*, 2590.
[27] K. Xu, *Chem. Rev.* **2004**, *104*, 4303.

© 2014 WILEY-VCH Verlag GmbH & Co. KGaA, Weinheim